TSINGHUA SCIENCE AND TECHNOLOGY
ISSN 1007-0214 11/12 pp294–301
DOI: 10.26599/TST.2019.9010016
Volume 25, Number 2, April 2020

Space and Frequency Diversity Characterization of Mobile GNSS Receivers in Multipath Fading Channels

Peirong Fan, Xiaowei Cui*, and Mingquan Lu

Abstract: Diversity reception of multipath Global Navigation Satellte System (GNSS) signals offers a new insight into carrier phase-based high-precision positioning. The focus of this paper is to demonstrate the fading independence between space and frequency diversity GNSS signals. In harsh urban environments, multipath components arrive to the mobile receiver antenna with different phases and Doppler shifts, therefore giving rise to the discontinuity of code and Doppler observations and large tracking errors. In this paper, an empirical model of fading GNSS signals is constructed, including power fluctuations and spread metrics. Based on this model, real BeiDou Navigation Satellite System (BDS) signals from two GNSS dual-frequency antennas are characterized, at both information and signal level. The block processing algorithm is utilized for signal investigation. Results show that: (1) a high proportion of asynchronous loss-of-lock (around 16%) is experienced by observations of diversity signals; and (2) power fluctuations of fading signals are uncorrelated in frequency separated branches unconditionally, yet for space diversity signals the independency exists in dynamic fading channels only. The results above corroborate the significant potential gain of diversity reception, and could be further implemented in researches of diversity combined GNSS parameter estimation in dense fading conditions.

Key words: Global Navigation Satellite System (GNSS); space/frequency diversity reception; power fluctuation; fading characterization

1 Introduction

Diversity reception of Global Navigation Satellite System (GNSS) signals provides a new research direction for the multipath fading issue of carrier phase-based high-precision positioning. In harsh urban environments, GNSS signals are undermined by constructive and destructive interference of multipath components on the Line-Of-Sight (LOS) signal[1]. This gives rise to ranging errors and measurement discontinuity[2]. However, researchers have noted that modern high-tech vehicles, such as drones and autopilot systems, are usually equipped with more than one antenna and receive on multiple frequencies for the purpose of GNSS-based attitude determination and ionosphere correction, respectively. This condition paves the way for space and frequency diversity researches, which aim at utilizing diversity combining techniques to improve GNSS tracking sensitivity and positioning robustness.

It is pivotal to explore the nature of diversity signals in dense fading environments because, theoretically, the less correlated the GNSS branches are, the greater the potential diversity gain will be. However, to the best of the authors' knowledge, the fading characterization of GNSS signal branches has rarely been discussed or corroborated.

Previous work on multi-antenna or multi-frequency reception has mainly focused on statistical model

• Peirong Fan, Xiaowei Cui, and Mingquan Lu are with the Department of Electronic Engineering, Tsinghua University, Beijing 100084, China. Peirong Fan is also with Beijing Satellite Navigation Center, Beijing 100094, China. E-mail: fpr09@foxmail.com; cxw2005@mail.tsinghua.edu.cn; lumq@mail.tsinghua.edu.cn.

∗ To whom correspondence should be addressed.

Manuscript received: 2019-01-01; accepted: 2019-04-15

constructions, which have been thoroughly researched in terms of the signal power distribution, Doppler spread and second-order statistics such as Level Crossing Rate (LCR) and Average Fade Duration (AFD)[3]. The power correlation coefficient between space-separated GNSS signals was quantified by Broumandan[4] with Rayleigh fading assumptions in 2009. For the ring of scatters multipath model, half a wavelength of separation is sufficient to ensure spatially uncorrelated signal samples[3]. Likewise, the power correlation coefficient between frequency-separated GNSS signals were formulated by Filho et al.[5] in 2005 with a sphere of scattering model. Under the assumption of Rayleigh fadings, several megahertz (MHz) of frequency separation is enough for signal decorrelation. However, the application of such models often depends on a myriad of assumptions, such as the fading environment and the relative dynamic between GNSS receivers and transmitters[6]. Therefore, the empirical model of real GNSS fading signals was introduced into GNSS power characterization by Sadrieh et al.[7] in 2012. Siddakatte et al.[1] examined the nature of real fading channels in high scattering indoor environments and dense urban canyons under limited dynamic range. The correlation coefficients between two fading channels with respect to power fluctuations and different characterization metrics were demonstrated therein.

However, there are two problems about characterizing fading signals that remain unsolved. On the one hand, fading signals have not been fully investigated in on-board mobile situations, which are frequently encountered by automatic driving vehicles. On the other hand, space and frequency separated signals are usually characterized in isolation, thus the diversity gain between those branches are disregarded.

In this paper, we focus on evaluating real fading signals received from mobile GNSS terminals and explore the multi-antenna and multi-frequency branches as a whole. To be specific, a combined diversity characterization of BeiDou Navigation Satellite System (BDS) fading channels is presented both at the information level and at the signal level. Raw observations and fading metrics (including Doppler spread, delay spread, and power fluctuation statistics) of BDS B1I and B2I signals from two space separated antennas are evaluated. A block processing technique[4] is utilized for signal observation. Results show that the measured probability of asynchronous loss-of-lock is high (around 16%) between diversity branches for a given satellite, and that the signal fadings are uncorrelated between frequency diversity branches, while for space diversity channels the more obvious fading irrelevance only appears in dynamic scenarios.

2 Fading Channel Empirical Model

2.1 Signal model

In urban canyon environments, the multipath GNSS signal received at antenna m is given as[7]

$$y_m(t) = r_m(t) + n_m(t) \tag{1}$$

where $n_m(t)$ denotes Additive White Gaussian Noise (AGWN), and $r_m(t)$ is the real GNSS signal, which can be expressed as

$$r_m(t) = \mathrm{Re}\left\{\sum_{k=0}^{K(t)}\left\{\begin{array}{l}\sqrt{2P_k(t)}d(t-\tau_k(t))c(t-\tau_k(t))\times\\ \exp[\mathrm{j}2\pi(f_c+f_{D,k}(t))(t-\tau_k(t))]\end{array}\right\}\right\} \tag{2}$$

where $d(\cdot)$ and $c(\cdot)$ are the navigation data message and the ranging code, respectively. P_k, τ_k, and $f_{D,k}$ are signal amplitude, code delay, and Doppler shift of the k-th multipath component, respectively. $K(t)$ is the total number of components at time t. $k = 0$ corresponds to the LOS component.

2.2 Characterization metrics

In order to construct the empirical model of GNSS fading channels, the following metrics are investigated:

(1) temporal Carrier-to-Noise Ratio (CNR),

(2) Doppler and delay spreads,

(3) LCR and AFD, and

(4) correlation coefficients of power fluctuations and spread metrics between different signal branches.

2.2.1 Doppler spread

The Doppler spread B_D is defined as the range of frequencies over which the received Doppler spectrum is essentially non-zero[8]. Statistically, it is negatively correlated with the time duration over which the channel impulse response is almost invariant[9]. In GNSS multipath fading channels, if the impulse response changes rapidly within the data duration, frequency dispersion due to Doppler spreading will occur, thus leading to signal distortion.

2.2.2 Delay spread

The delay spread σ_τ describes the variation in the propagation delays of multiple scattered signals. In general, it is negatively correlated with the range of

frequencies over which the channel can be considered to pass all the frequency components with almost equal gain and linear phase[10]. With the knowledge of true Doppler $\overline{f}_D$, the Root-Mean-Square (RMS) delay spread is defined as

$$\sigma_\tau = \sqrt{\frac{\sum_k R(\overline{\tau}_k|\overline{f}_D)(\tau_k - \tau_{\text{mean}})^2}{\sum_k R(\overline{\tau}_k|\overline{f}_D)}} \tag{3}$$

where $R(\overline{\tau}_k|\overline{f}_D)$ represents the Cross Ambiguity Function (CAF) with known Doppler $\overline{f}_D$. $\tau_{\text{mean}} = \left(\sum_k R(\overline{\tau}_k|\overline{f}_D)\tau_k\right) \Big/ \left(\sum_k R(\overline{\tau}_k|\overline{f}_D)\right)$ is the mean excess delay.

2.2.3 LCR and AFD

LCR and AFD are second-order statistics of the signal power, which are utilized to assess the severity of the fading over time. LCR is the average number of crossings per second at which the GNSS signal envelope crosses a specified level with positive slope. With a specified threshold level L, LCR N_L can be expressed as[10]

$$N_L = \int_0^\infty \dot{x}\, p(L, \dot{x}) \mathrm{d}\dot{x} \tag{4}$$

where $\dot{x}$ is time derivative of signal envelope x, $p(L, \dot{x})$ is the joint Probability Density Function (PDF) of x, and $\dot{x}$ is computed at $x = L$.

The AFD A_L is defined as the average period of time during which the signal power is below level L[10],

$$A_L = \frac{\sum_k t_k}{N_L T} \tag{5}$$

2.2.4 Correlation coefficient

The linear correlation of characterization metrics between two signal branches are measured with the correlation coefficient[11, 12],

$$\rho = \frac{E(X_1 X_2^*)}{E(X_1 X_1^*)E(X_2 X_2^*)} \tag{6}$$

where X_1 and X_2 are zero mean random variables, X^* is the conjugate transpose of X, and $E(\cdot)$ represents the averaging function. The parameter ρ has a value between 0 and 1, where 1 is total linear correlation.

3 Block Processing Algorithm

Figure 1 shows the block diagram of a coherent block processing algorithm. As can be seen, external data bits are extracted to process signal blocks longer than 1 ms (length of one BDS NH code). BDS signal

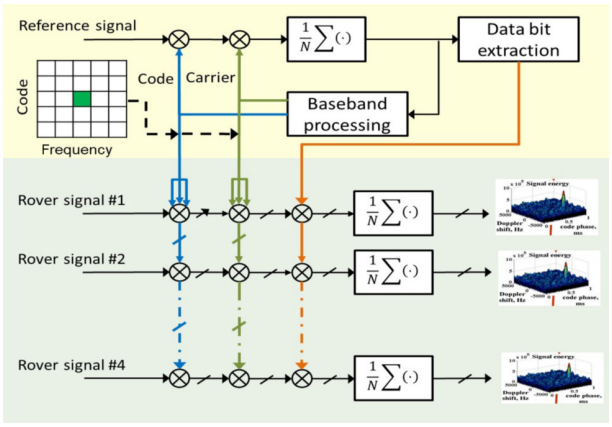

Fig. 1 Block diagram of the coherent block processing algorithm.

blocks are coherently correlated with the replica signal for all possible discrete values of Doppler and code phases, and a bank of correlators for each processing epoch are realized[11]. Parameters for each epoch are estimated independently. The objective of coherent integration is to avoid the CNR degradation caused by non-coherent square loss. Doppler and code phase reference in Fig. 1 are calculated by a high-precision post-processing receiver.

In the measurement of fading metrics, the CAF $R(\tau, f_D)$ can be generated through a 2-dimension search[5] over the delay-frequency vector $\hat{\boldsymbol{a}} = (\hat{\tau}, \hat{f}_D)$. Based on the signal model above, we obtain the expression of $R(\tau, f_D)$ as

$$R(\hat{\tau}, \hat{f}_D) = \sum_{n=0}^{L-1} \Big\{ y_m(t) c(nT_s - \hat{\tau}) \times \exp[-\mathrm{j}2\pi(f_{IF} + \hat{f}_D) n T_S] \Big\} \tag{7}$$

where nT_s is the discrete form of t, and L represents the integration time. The envelope of $R(\hat{\tau}, \hat{f}_D)$ is evaluated in a grid on points $\tau_s = s \cdot \Delta\tau$ and $f_{l,D} = l \cdot \Delta f_D$, where $\Delta\tau$ is the delay bin size and Δf_D is the Doppler bin size. The Maximum Likelihood (ML) estimation of $\hat{\boldsymbol{a}}$ is

$$\hat{\boldsymbol{a}}_{\text{ML}} = \arg\min_{\hat{\boldsymbol{a}}} |R(\hat{\tau}, \hat{f}_D)|^2 \tag{8}$$

4 Data Collection

In this paper, real BDS signals were collected with two omnidirectional GPS500 antennas on B1I and B2I frequencies (centered on 1561.098 MHz and 1207.14 MHz, respectively) in Tsinghua University, China. Figure 2 illustrates the test set-up. The antennas were placed 40 cm apart. Raw BDS signals on each antenna were split into two branches, one of which was

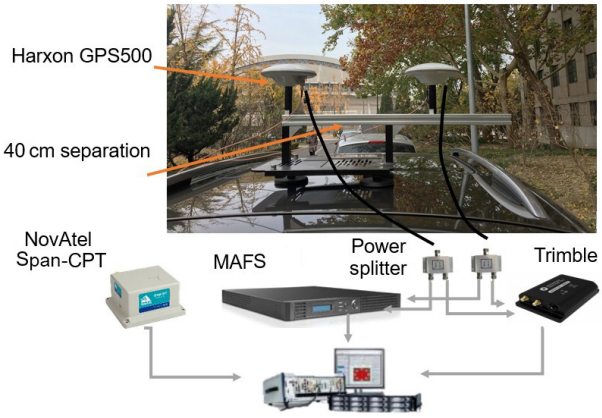

Fig. 2 Test set-up for real BDS data collection.

connected to a Trimble multi-frequency GNSS receiver while the other was connected to a self-developed Multi-Antenna multi-Frequency data Sampling system (MAFS). The assisting navigation data were collected with NovAtel Span-CPT, a high-precision GNSS/INS integrated receiver, which was firmly mounted on the rooftop of the Weiqing building.

In this regard, the objective of raw BDS observations from the Trimble is for fading comparison at the level of GNSS information. The baseband data from MAFS are aimed at evaluation at the level of signals.

Two sets for BDS data were collected, one in a static and one in a dynamic dense fading environment. Figure 3 shows the static multipath environment and the sky plot of Data Set-I. Figure 4 depicts the dynamic fading scenario and the vehicle trajectory. Satellite visibility and elevations are listed in Table 1. In this paper, medium and high elevation satellites, including BDS Pseudo Random Noise code (PRN) 6, 9, 13, and 16, are characterized as low elevation satellites are usually eliminated in Real-Time Kinematic (RTK)-based positioning.

4.1 Noise calibration

The thermal noise in Trimble observations and MAFS RF channels was calibrated by connecting the two

(a) Fading scenario of Data Set-I (b) Sky plot of medium and high elevation satellites

Fig. 3 Static fading environment and sky plot (Data Set-I).

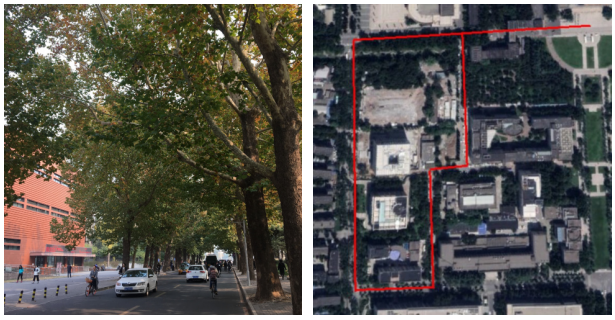

(a) Fading scenario of Data Set-II (b) Field test trajectory in Tsinghua University

Fig. 4 Dynamic fading environment and field test trajectory (Data Set-II).

Table 1 Data collection details.

Environment	Antenna dynamics	Signal visibility PRN (elevation)
Data Set-I Urban canyon, GW Hall, THU, 6th Nov 2018, 5:57 am UTC	Static: 5 min	PRN 6 (77.3°) PRN 13 (57.0°) PRN 9 (52.7°) PRN 16 (49.1°)
Data Set-II Urban canyon, THU, 6th Nov 2018, 5:43 am UTC	Kinematic: Average speed ∼6 m/s, 6 min	PRN 6 (77.9°) PRN 13 (59.6°) PRN 9 (52.2°) PRN 16 (48.2°)

power splitters in Fig. 2 to the same antenna, which was firmly mounted on the open rooftop of the Weiqing building of Tsinghua University. Standard CNR deviations of two BDS signal branches, denoted by capital letters A and B, respectively, are listed in Table 2. As can be seen, the maximum CNR fluctuation is smaller than 0.5 dB (1σ) for the Trimble receiver and smaller than 1.0 dB (1σ) for the MAFS RF channels.

5 Characterization Results

In this section, raw observations from the mobile Trimble receiver are firstly compared between branches at the level of navigation information. After that two

Table 2 Standard deviation of CNR in Trimble and MAFS platforms.

(dB)

	PRN	B1I_A	B2I_A	B1I_B	B2I_B
Trimble	6	0.39	0.34	0.33	0.42
	9	0.24	0.32	0.29	0.29
	13	0.25	0.29	0.25	0.46
	16	0.35	-	0.28	0.43
MAFS	6	0.76	0.70	0.86	0.68
	9	0.92	0.65	0.77	0.72
	13	0.69	0.73	0.78	0.74
	16	0.77	0.71	0.81	0.67

sets of BDS baseband signals from the MAFS are evaluated at the signal level.

5.1 Observations usability

Figure 5 depicts the number of satellites visible in the B1I and B2I branches of antennas rover1 and rover2, respectively.

A fairly close and substantially constant number of satellites for all space and frequency separated BDS signals are revealed at the beginning and the end of the data set when the vehicle was stationary.

However, a significant fluctuation of visible satellites appeared when the vehicle started moving. Dissimilar variation trends can be seen throughout the test. For example, at time $t_1 = 44:49$, even though both rover1_B1I and rover1_B2I signals could see no more than 5 satellites, which is the minimum observations required for RTK ambiguity resolution, the rover2 B1I and B2I branches were able to track 6 satellites. This situation reversed at time $t_2 = 46:20$, when rover1 branches could see 2 or 3 more satellites than rover2 branches. In fact, the situation appeared at time $t_3 = 44:48$ is more common, when only one of the four branches could see 5 or more satellites.

In addition, at the upper right corner of Fig. 5 is listed the statistical visibility of a certain satellite (PRN 9) in all four diversity branches. It can be seen that for around 16% of the entire epochs, BDS observations are asynchronously usable in the four diversity channels.

5.2 Fading characterizations

Essentially, the inferior usability of the GNSS observations above results from the significant power fluctuations of the fading signal. In this regard, this paper investigated real BDS signals with the following metrics, according to the empirical model presented in Section 2.2.

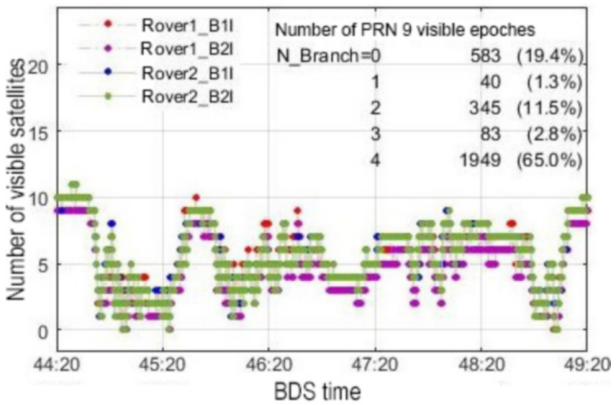

Fig. 5 Number of visible satellites and observation usability of PRN 9 of the GNSS receiver.

5.2.1 Instantaneous power fluctuation

Figure 6 shows the instantaneous CNR fluctuations of diversity branches in Data Set-I for PRN 9, 13, and 16; the signal power varies to the order of a few dB and the variation trend is similar between branches, even though the receiver suffered from dense fading conditions.

Figure 7 shows the CNR fluctuations of Data Set-II, revealing great fading depths as deep as 26 dB, and that the power difference between low and deep fading branches reaches 20 dB at most.

The power correlation coefficient between each pair of space and frequency separated branches are listed in Table 3. As shown in Table 3, the spatial

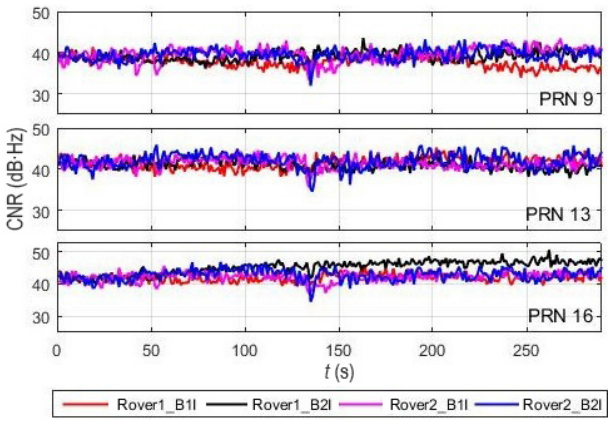

Fig. 6 CNR fluctuations of frequency and space diversity branches in Data Set-I.

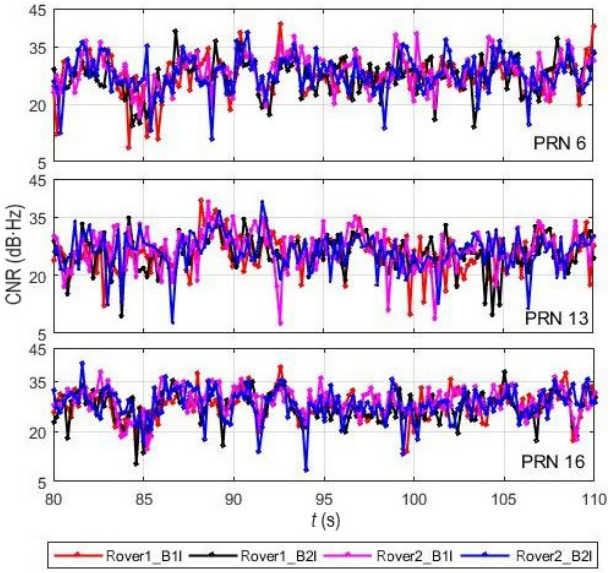

Fig. 7 CNR fluctuations of frequency and space diversity branches in Data Set-II.

Table 3 Power correlation coefficients between diversity branches.

Data set	PRN	Space separated		Frequency separated	
		B1I_A vs B1I_B	B2I_A vs B2I_B	B1I_A vs B2I_A	B1I_B vs B2I_B
I	6	-	0.96	0.0013	-
	13	0.96	0.97	0.0010	0.0015
	16	0.95	0.93	0.0000	0.0013
	9	0.94	0.98	0.0005	0.0011
II	6	0.18	0.28	0.0009	0.0018
	13	0.28	0.68	0.0020	0.0015
	16	0.20	0.20	0.0014	0.0014
	9	0.16	0.66	0.0014	0.0029

Note: Correlation coefficients of PRN 6 in channel B1I_B of Data Set-I is unavailable due to a tracking failure.

diversity signals received on the same frequency are strongly correlated in Data Set-I. The correlation coefficients are greater than 0.9. However, significant independence appeared in dynamic scenarios, where the correlation coefficients plummeted to below 0.3. By contrast, power fluctuations in frequency diversity signals received at the same antenna are almost absolutely uncorrelated, as the correlation coefficients are on the order of 0.001. This uncorrelation appeared under both static and dynamic conditions.

5.2.2 Doppler and delay spread

Figure 8 demonstrates the measured PDF of the Doppler spread, as observed by four diversity branches in Data Set-II. The coherent integration time (Tcoh) is 400 ms, and the Doppler resolution Δf is 2.5 Hz.

It can be seen that the statistical distribution is similar in different branches. The Doppler spread range is within 20 Hz. The measured fading coherent time, which is the inverse of the Doppler spread, is greater than 50 ms. Within this time period, the transfer function at a given signal frequency can be regarded as time-irrelevant.

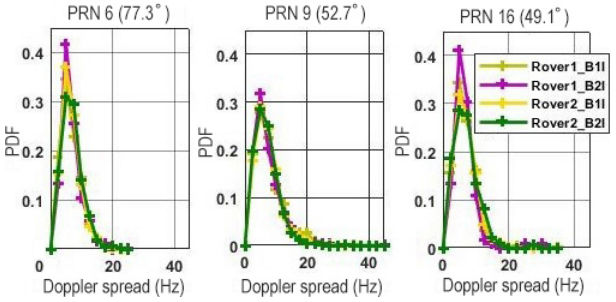

Fig. 8 Doppler spread of fading diversity branches in Data Set-II (Tcoh=400 ms, Δf =2.5 Hz).

Figure 9 shows the correlation coefficients of instantaneous Doppler error between space and frequency diversity branches. The Doppler reference was obtained from a high-precision post-processing receiver. For medium and high elevation satellites, the Doppler error experienced by two spatially separated antennas is moderately correlated. For frequency separated signals, this correlation decreased somewhat.

Figure 10 shows the measured PDF of the delay spread in Data Set-II. The spread range is in the order of nanoseconds, meaning that the coherence bandwidth of the fading channel, which is the inverse of the delay spread, is much larger than the signal bandwidth. Therefore, different signal frequency components will pass the channel with almost equal gain and linear phase.

Correlation coefficients of the delay error showed a similar low dependency between fading branches.

5.2.3 LCR and AFD

Figure 11 shows the LCR and AFD plots for the static and dynamic situations. It can be seen that, under static conditions, the change of the LCR curve with the CNR threshold is a standard belly shape, indicating that the signal amplitude does not fluctuate significantly, and the corresponding AFD curve is monotonically increasing. However, under dynamic conditions, flat

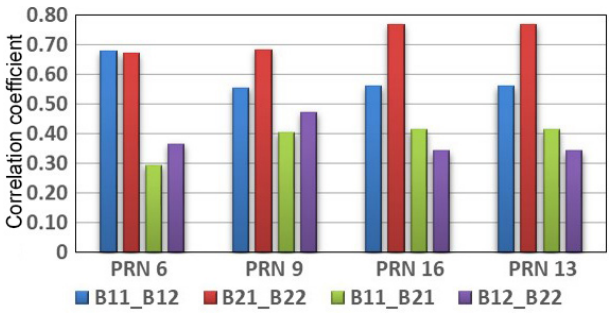

Fig. 9 Doppler error correlation coefficients of fading diversity branches in Data Set-II.

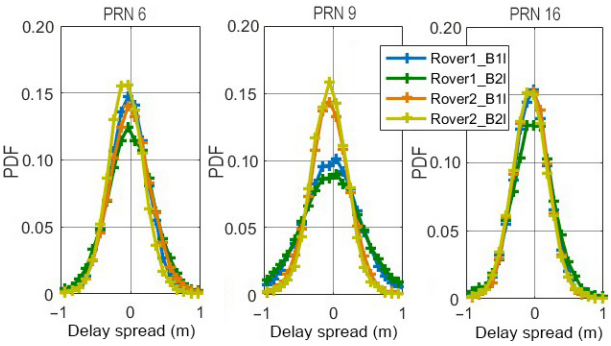

Fig. 10 Delay spread of fading diversity branches in Data Set-II (Tcoh=20 ms).

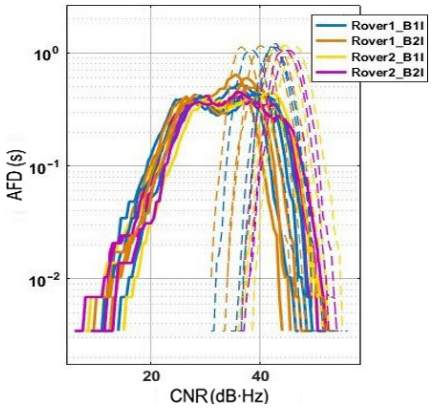

(a) LCR

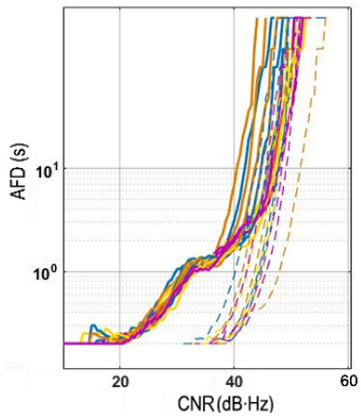

(b) AFD

Fig. 11 LCR and AFD for static and dynamic fading environments.

intervals appeared in both LCF and AFD curves. The wider the interval, the more severe the power fluctuation. Similar to spread metrics, the statistical characteristics of the power variation of each branch are similar, which is motion-irrelevant.

5.3 Summary of results

Three characteristics can be obtained from the analysis above:

(1) Situations exist in which each signal branch failed to track enough number of satellites for GNSS positioning on its own, but the combined system could see more than 5 satellites;

(2) CNR fluctuations are deep (reaching 26 dB), but are un-correlated between space and frequency separated branches under dynamic scenarios; and

(3) Navigation parameters in diversity branches are strongly statistically correlated.

6 Conclusion

In this paper, an empirical model of BDS fading signals has been constructed. Diversity characterizations of real BDS dual-antenna and dual-frequency signals under dynamic and static dense fading environments are evaluated. Results show that: (1) at the information level, the diversity reception gain is corroborated by asynchronized loss-of-lock of signal branches; and (2) at the signal level, the combination gain has been demonstrated by the fading independence of diversity signals.

In conclusion, making full use of the fading independency between diversity signal branches is of great importance for mobile high-precision navigation in GNSS-challenged environments, which becomes the focus of our future research.

References

[1] R. K. Siddakatte, A. Broumandan, and G. Lachapelle, Enhanced GNSS signal tracking in fading environments using frequency diversity, *Navigation: Journal of the Institute of Navigation*, vol. 64, no. 2, pp. 213–229, 2017.

[2] T. S. Rappaport, *Wireless Communications: Principles and Practice*. Englewood Cliffs, NJ, USA: Prentice Hall PTR, 1996.

[3] R. K. Siddakatte, Enhanced GNSS signal tracking in fading environments using diversity reception, PhD dissertation, University of Calgary, Canada, 2016.

[4] A. Broumandan, Enhanced narrowband signal detection and estimation with a synthetic antenna array for location applications, PhD dissertation, Department of Geomatics Engineering, University of Calgary, Canada, 2009.

[5] C. S. S. Filho, G. Fraidenraich, U. S. Dias, and M. D. Yacoub, On the Nakagami-m crosscorrelation function, presented at the Proc. SBMO/IEEE MTT-S International Microwave and Optoelectronics Conference 2005, Brazilia, Brazil, 2005.

[6] S. J. P. T. Satyanarayana, GNSS channel characterization and enhanced weak signal processing, PhD dissertation, University of Calgary, Canada, 2011.

[7] S. N. Sadrieh, A. Broumandan, and G. Lachapelle, Doppler characterization of a mobile GNSS receiver in multipath fading channels, *Journal of Navigation*, vol. 65, no. 3, pp. 477–494, 2012.

[8] L. L. Presti, X. Zhu, M. Fantino, and P. Mulassano, GNSS signal acquisition in the presence of sign transition, *IEEE Journal of Selected Topics in Signal Processing*, vol. 3, no. 4, pp. 557–570, 2009.

[9] D. Borio, N. Sokolova, and G. Lachapelle, Doppler measurement accuracy in standard and high-sensitivity global navigation satellite system receivers, *IET Radar Sonar and Navigation*, vol. 5, no. 6, pp. 657–665, 2011.

[10] E. Kaplan and C. Hegarty, *Understanding GPS: Principles and Applications*. Norwood, MA, USA: Artech House, 2005.

[11] M. Ibnkahla, *Signal Processing for Mobile*

Communications Handbook. Boca Raton, FL, USA: CRC Press, 2004.

[12] S. T. Garren, Maximum likelihood estimation of the correlation coefficient in a bivariate normal model with missing data, *Statistics & Probability Letters*, vol. 38, no. 3, pp. 281–288, 1998.

Peirong Fan received the BS degree from Tsinghua University, China, in 2013. She is currently a PhD student at Tsinghua University. Her research focuses on high sensitivity Global Navigation Satellite System (GNSS) signal tracking and robust RTK positioning in urban fading environments.

Xiaowei Cui received both the BS and PhD degrees from Tsinghua University in 1999 and 2004, respectively. He is an associate professor at the Department of Electronic Engineering, Tsinghua University, China. He is a member of the expert group of China BeiDou Navigation Satellite System. His research interests include robust GNSS signal processing, multipath mitigation techniques, and high-precision positioning.

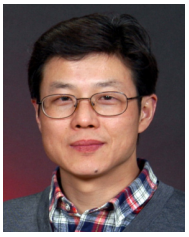

Mingquan Lu received the MS degree from the University of Electronic Science and Technology of China in 1993. He is a professor of the Department of Electronic Engineering, Tsinghua University, China. He is the director of Tsinghua Position, Navigation and Timing Center, and a member of the expert group of China BeiDou Navigation Satellite System. His current research interests include GNSS signal design and analysis, GNSS signal processing and receiver development, and GNSS system modeling and simulation.